Ultrafiltration of non-spherical molecules

Aguirre Montesdeoca, V., Bakker, J., Boom, R. M., Janssen, A. E. M., & van der Padt, A.

Ultrafiltration of non-spherical molecules

Victor Aguirre Montesdeoca*[1,2], Jaap Bakker[2], R. M. Boom[2], Anja E. M. Janssen[2], and A. Van der Padt[2,3].

[1]Institute for Sustainable Process Technology, P.O. Box 247, 3800 AE, Amersfoort, The Netherlands.

[2]Wageningen University, Food Process Engineering Group, P.O. Box 17, 6700 AA, Wageningen, The Netherlands.

[3] FrieslandCampina, P.O. Box 1551, 3800 BN, Amersfoort, The Netherlands.

*Corresponding Author: E-mail: victor.aguirremontesdeoca@wur.nl

ABSTRACT

Information about the sizes of the solute molecules and membrane pores is needed to estimate solute rejection in filtration processes. Molecules are normally regarded as spheres, and the Stokes radius is commonly used to represent their molecular size. However, many molecules used in food and pharma processes are oligomers or polymers which are strongly elongated; therefore, considering them spherical affects the accuracy of the model predictions.

We here adapt the so-called Steric Pore Model to a more realistic representation of the transfer of rigid elongated molecules into and through ultrafiltration membrane pores. To do so, sugars with different degree of polymerization were used as model molecules. They were considered to be capsule-shaped to facilitate their size estimation. In order to represent the system as accurately as possible, the effect of hydration on the sugars size was included, and the membrane pore size distribution was estimated based on rejection data.

It was demonstrated that considering these molecules to be capsule-shaped instead of spherical generates better predictions over the entire rejection spectrum using a unique pore size distribution. Additionally, this capsular geometry lets us simplify the calculations, making the estimation of the rejection straightforward.

Keywords: capsule-shaped molecules; pore size distribution; oligosaccharides; elongated molecules; hydration of sugars.

1. Introduction

Filtration technology have gained popularity in the food and biotechnology industry in the last decades due to its simplicity, low costs and sustainable features [1]. Together with this increase in popularity, the need of a mathematical representation for these processes has emerged. Disciplines such as Process Design, Process Optimization and Process Control require a mathematical representation of the system to proceed. Additionally, the convenience of knowing in advance the outcome of a separation, without actually performing it, is unquestionable. Therefore, many efforts have been done in the last 30 years to understand and model these processes.

When modelling ultrafiltration (UF), two main methods can be distinguished: The 'Black Box' method, in which phenomenological equations based on non-equilibrium thermodynamics are used [2, 3], and the so-called Steric Pore Model (SPM), which is a more mechanistic model, that has been improved and modified over the years [4, 5]. Both methods require preliminary experiments for the estimation of parameters that later on are used to predict the behaviour of the system under different process conditions [6]. The SPM model has the advantage that it is more adaptable and the estimated parameters have a clear physical meaning, making them easier to grasp and relate.

UF modelling comprises the representation of the mass transfer outside and inside the membrane. Thus, information about the physical dimensions and properties of the transient solute molecules and the membrane pores is needed to mathematically represent the solute rejection. To simplify this representation, solute molecules are normally regarded as spheres, using the Stokes radius (r_S) as a measure of their molecular dimension. For non-spherical molecules, however, this simplification produce large deviations in the calculation of the solute rejection [7].

Many molecules used in food and pharma processes are oligomers or polymers with a strongly elongated shape. For this type of molecules chain flexibility is a critical factor that determines their hydrodynamic properties [8-10]. Fortunately, small chains (oligomers) can normally be considered rigid, facilitating their representation, since they can be can be regarded as a continuous capsule-shaped body[9]. This capsular geometry (cylinders bounded along the edges by semispherical surfaces) is also referred as 'spherocylinders' by other authors [8].

Some efforts have already been made to consider the actual shape of elongated solute molecules in the modelling of their rejection in membrane pores. Their shape have been approximated to different geometries such as cylinders [7, 11], rectangular parallelepipeds [12, 13] and spheroids [14, 15]. In order to condense the molecular dimensions of such molecules in one unique parameter, Van der Bruggen et al. calculated an 'Effective diameter' based on the dimensions obtained after the minimisation of the molecular energy in the three-dimensional configuration of the molecules [7, 11]. Similarly, Kiso et al, estimated the 'Molecular width', which was found to be more appropriate than r_S for the modelling of the rejection [12, 13]. These methods, however, require the use of sophisticated software to model the 3D structure of each solute molecule. Additionally, these studies consider the bare molecule *in vacuo*, without considering any interaction with the solvent (such as hydration). Therefore, more convenient and better methods are needed to model the UF of elongated molecules while keeping the problem complexity low. Preferably, these methods should use input parameters that are readily available in the literature or can be determined easily.

We here report on the adaptation of the existing ultrafiltration theory (SPM model) to a more realistic representation of the mass transfer of rigid elongated molecules through membrane pores. To do so, sugars with different degree of polymerization (DP) were used as model molecules, which were considered to be capsule-shaped to facilitate their size estimation. For accurate predictions, the effect of hydration on the sugars size was included, while the membrane pore sizes were assumed to follow a log-normal distribution.

2. Theory

2.1 Solute molecules as capsules

The exclusion of an uncharged non-interacting solute molecule is entirely due to the steric constraints of the pore wall. An excluded volume originates near the pore wall where the centre of solute molecules cannot access because of their finite dimensions [16]. It is generally assumed that the membrane pores are perfect cylinders and that the solute molecule is a perfect sphere. As shown in Eq. 1, under these conditions the calculation of a partition coefficient (Φ) at the membrane interface is straightforward, being a function of the radius of the pore (r_p) and the radius of the spherical molecule (r_i) [17].

$$\Phi = \left(1 - \frac{r_i}{r_p}\right)^2 \tag{1}$$

For modelling purposes, r_i is commonly represented with r_S, which, by definition, is the radius of a sphere of equal diffusivity as that of the solute molecule. r_S can be calculated from the bulk diffusivity as shown in Eq. 2 [18]. Evidently, the simplification $r_i = r_S$ loses accuracy as the molecule shape departs from sphericity.

$$r_S = \frac{k_B T}{6\pi\eta D} \tag{2}$$

In a study of exclusion chromatography, Giddings et al. assessed the effects of different molecular shapes on the partition coefficient Φ in pores of different geometries. In the case of elongated molecules, the calculation of Φ in the pore interface turns into a complex problem where molecular orientation and position play an important role [16, 19]. They found that it is more convenient to represent elongated molecules as capsules rather than as spheroids [16]. While the interested reader is advised to read the original paper for a more detailed explanation, we will here give a summary of the reasoning.

In the case of a capsule-shaped molecule and a cylindrical pore, Φ can be considered to be the configuration–space average of the probability q of no intersection with pore walls (Eq. 3).

$$\Phi = \frac{\iint q(p,\psi)\, dpd\psi}{\iint dpd\psi} = \frac{\int \varphi'(p)dp}{\int dp} = \frac{\int \varphi''(\psi)d\psi}{\int d\psi} \tag{3}$$

where p and ψ are generalized coordinates that describe the position and the orientation of the molecule respectively. Likewise, the local partition coefficients ($\varphi' \; and \; \varphi''$) can be defined as shown in Eq.4 and 5.

$$\varphi'(p) = \frac{\int q(p,\psi)d\psi}{\int d\psi} \tag{4}$$

$$\varphi''(\psi) = \frac{\int q(p,\psi)dp}{\int dp} \tag{5}$$

Given a molecule with a specific p and ψ, the probability q that this molecule is not intersected by a pore wall is going to be 1 or 0. Evidently, the restraints imposed by the pore wall will reduce the concentration of solutes near the wall. Additionally, since the surface of the cylindrical pore is assumed to have axial symmetry, ψ can be simply represented by the angle (θ) of the molecular axis with respect to the pore axis.

The size of a capsule-shaped molecule can be represented by its length $L_1$and its width (which is equal to its depth) L_0. Thus, parameters r_1 and r_0 can be defined as the half of L_1 and L_0 respectively. While r_0 represents the radius of the spherical caps at the sides of the capsule, r_1 is not a radius but the half-length. As a limiting case, Giddings et al. derived expressions for Φ and φ'' when the molecule is a rod with an infinitely small thickness ($r_0 = 0$). Since rods have only one dimension (r_1) the resulting equations are straightforward to solve.

$$b = \sqrt{{r_p}^2 - {r_1}^2 \, sin^2\theta} \tag{6}$$

$$\varphi'' = \frac{4}{{r_p}^2\pi}\int_0^b \left(\sqrt{{r_p}^2 - p^2} - r_1 sin\theta\right) dp \quad (r_1 sin\theta \le r_p;\; otherwise\; \varphi'' = 0\,) \tag{7}$$

$$\Phi = \frac{\int_0^{\pi/2} \varphi'' sin\theta \, d\theta}{\int_0^{\pi/2} sin\theta \;\; d\theta} = \int_0^{\pi/2} \varphi'' sin\theta \, d\theta \tag{8}$$

The limiting case represented in Eqs.6, 7 and 8 is useful because the area available for the centre of a capsule-shaped molecule (with dimensions r_1 and r_0) in a pore with radius r_p is the same as the available area for the centre of an infinitely thin rod ($r_0 = 0$) with a half-length equal to $r_1 - r_0$ in a pore with radius $r_p - r_0$ (Figure 1). As consequence, by defining two new parameters $\hat{r_1} = r_1 - r_0$ and $\hat{r_p} = r_p - r_0$ and using them in the aforementioned equations, a value for $\Phi(\hat{r_1}, \hat{r_p})$ can be calculated. This value is still not equal to $\Phi(r_1, r_p)$ since the free volume in the pore is higher with r_p as the radius of the pore. The final correction can be done as shown in Eq. 9.

$$\Phi = \frac{(r_p - r_0)^2}{{r_p}^2} \Phi(\hat{r_1}, \hat{r_p}) \tag{9}$$

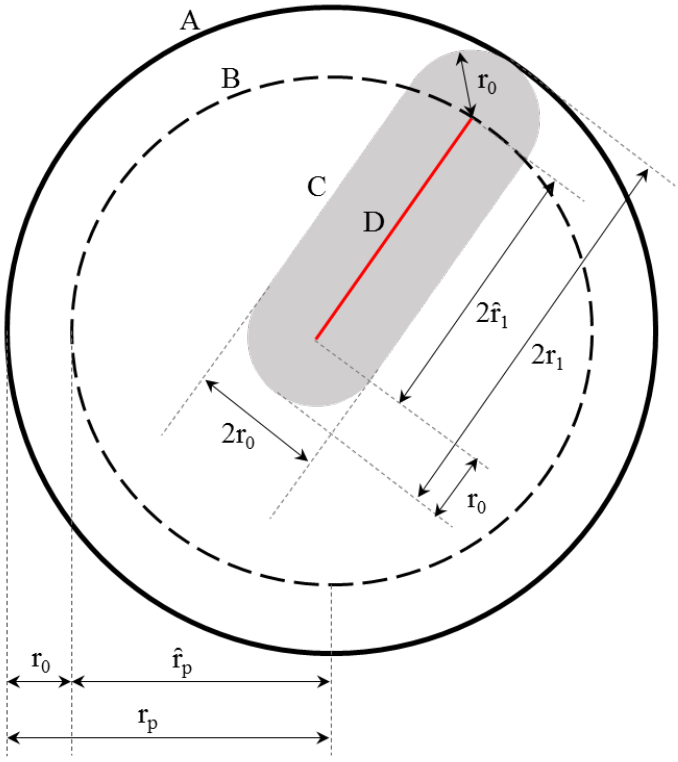

Figure 1. Representation of equivalent free available pore area for an infinitely thin rod D in pore B and capsule C in pore A. The dimensions of the rod are $\widehat{\boldsymbol{r_1}} = \boldsymbol{r_1} - \boldsymbol{r_0}$ and $\widehat{\boldsymbol{r_0}} = \boldsymbol{0}$ while the dimensions of the capsule are $\boldsymbol{r_1}$ and $\boldsymbol{r_0}$.

As shown in Figure 1, this methodology is specially suitable for capsules. Additionally Giddings et al. found empirically that one could obtain a good estimation of Φ by calculating an Average radius (r_G),

based on the two values that define a capsule r_1 and r_0 (Eq. 10). Thus, considering r_G as a dimensional parameter and using Eq.1, as if the molecule would be spherical, can also lead to straight forward approximations of Φ for capsule-shaped molecules.

$$r_G = \frac{r_1 + r_0}{2} \tag{10}$$

Apart from the convenience in the calculation of Φ, one extra advantage of considering elongated molecules to be capsules is the suitability, in the case of chain-like molecules, of calculating their dimensions from information about their monomers as it is explained in section 2.2.

2.2 Hydration of molecules

The interaction of solute and solvent molecules influences the physical properties of the solution and the effective dimension of the solute molecules. For sugars, the proximity of many hydroxyl moieties suggests that the molecular properties of water are critical for an understanding of the structure and dynamics of the sugars [20]. Hence, each sugar molecule and the water in its hydration layer will be regarded as a whole.

The hydration of a sugar can be estimated by the method of Gharsallaoui et al. (2008), which uses density data of single sugar solutions and hydration numbers from literature to estimate the hydrated molar volume (V_m) of the sugar [21]. Once this is done for the monosaccharides of interest, their radii can be calculated by considering them to be spherical. Subsequently, the length and width of the whole capsular oligosaccharide can be estimated by aligning the spherical monosaccharides next to each other as represented in Figure 2, assuming that the volume of each moiety remains equal. L_1 (the length) is equal to the sum of all the diameters of the monosaccharides in the capsule, while L_0 (the width and depth) is represented by the diameter of the bigger monosaccharide in the chain. Hence, V_m for the oligosaccharides is the sum of the V_m values of the individual monomers.

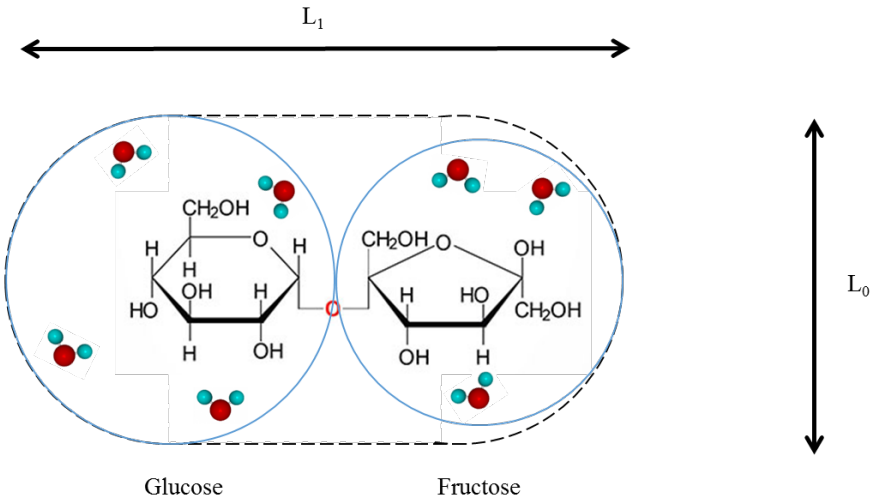

Figure 2. Representation of the sucrose molecule as a capsule composed by two spherical monomers, in which $\boldsymbol{L_1}$ represents the length of the molecule and $\boldsymbol{L_0}$ is the depth and the width of the molecule.

The structural considerations explained above are valid as long as an extended configuration for the chain is assumed. For disaccharides, this is true by definition. In the case of longer oligosaccharides, this assumption is not far from reality considering that these molecules tend to remain rigid and extended when they are in solution [20, 22, 23]. Almond et al. studied the structure of many oligosaccharides using molecular dynamics simulations and NMR measurements, and found that the interactions between the water molecules and the sugars result in tight and ordered conformations [23]. Later, they found that the presence of β linkages determine extended and relatively rigid structures that resulted in an end-to-end distance close to maximum [20, 22].

2.3 Fructooligosaccharides

Fructooligosaccharides are short chains of D-fructose units linked by β(2-1) bonds that may carry a terminal α(1-2) linked D- glucose [24]. For modelling purposes this mixture of GF_n and F_n molecules can be classified according to their DP. Additionally, it is important to consider the peculiar behaviour of fructose. When fructose is in solution, its pyranose configuration (six-membered ring) is dominant [25]. However, when fructose is part of a chain, as it is the case in fructooligosaccharides, it assumes its furanose configuration (five-membered ring) [26]. Therefore, the volume of the hydrated fructose molecule in the oligosaccharide chain is smaller than its volume in its free form. The volume of this

‘chained fructose’ can be estimated by subtracting the volume of a hydrated glucose molecule from the hydrated volume of sucrose. Table 1 shows the estimated hydrated properties of some simple sugars used in this study.

Table 1. Hydration data of different sugars estimated according to Gharsallaoui et al. [21]. $\boldsymbol{r_1}$ and $\boldsymbol{r_0}$ represent the half-length and the radius of the spherical caps at the sides of the capsule-shaped molecule, respectively.

Molecule	Hydration number ($\boldsymbol{n_H}$)	Molar volume (bare molecule) [10^{-6} m^3/mol]	Molar volume (Hydrated molecule) [10^{-6} m^3/mol]	$\boldsymbol{r_1}$ [10^{-10} m]	$\boldsymbol{r_0}$ [10^{-10} m]
Xylose	2.3[27]	98.7	139.8	3.81	3.81
Glucose	3.5[27]	118.1	174.8	4.11	4.11
Fructose	3.8[27]	118.0	179.2	4.14	4.14
Fructose in chain			128.3	3.70	3.70
Sucrose	5[21]	221.0	303	7.81	4.11
Raffinose			478	11.92	4.11

The dimensions of elongated molecules can be represented in three different ways: (1) the molecules can be considered to be spherical and the Stokes equation (Eq. 2) can be used to estimate their r_S ; (2) the molecules can be considered to be capsules and an average radius r_G according to Eq. 10 can be estimated in what we have called a Simplified Capsular approach; or (3) a Complete Capsular approach can be used, in which the molecular dimensions are represented by the two parameters that define a capsular geometry: r_1 and r_0. Figure 3 shows the oligosaccharides’ estimated dimensions using these 3 approaches based on the data in Table 1. Notice that all three approaches are equivalent for the case of monosaccharides, which can be regarded as spherical molecules. This means that considering molecular hydration in the solutes size improves the reliability of the approach since similar radii are calculated from diffusion (r_S) and density data (r_G).

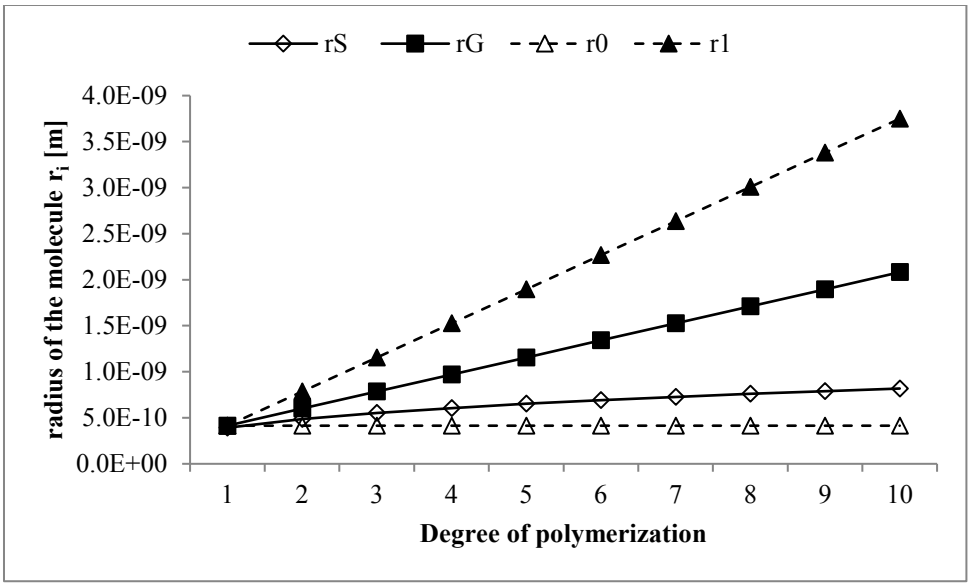

Figure 3. Radii of fructooligosaccharides as function of their degree of polymerization according to three different approaches: Spherical ($\boldsymbol{r_S}$), Simplified Capsular ($\boldsymbol{r_G}$) and Complete Capsular ($\boldsymbol{r_1}$, $\boldsymbol{r_0}$). Only the symbols are produced by the calculations; lines were drawn to guide the eye.

2.4 Mass transfer outside the membrane

To estimate the mass transfer in the concentration polarization layer, the classic film model can be used (Eq. 11). In this way, an experimental Real Rejection (R) can already be calculated as shown in Eq. 12.

$$C_m = (C_r - C_p)\, exp\left(\frac{J}{k}\right) + C_p \tag{11}$$

$$R = 1 - \frac{C_p}{C_m} \tag{12}$$

For very diluted solutions, where the osmotic pressure difference over the membrane can be neglected, the permeate flux (J) is a linear function of the pressure $|\Delta P|$, where the slope of this line is the membrane permeability (L_p) as shown in Eq. 13.

$$J = L_p\, |\Delta P| \tag{13}$$

The mass transfer coefficient k can be calculated using the Sherwood expression for spiral wound modules presented by Schock and Miquel[28]. They obtained this relation from experimental filtration data with different membranes, spacers and pressures, the Sherwood equation presented below can be considered to already contain suction effects due to the flux through the membrane [29].

$$k = \frac{Sh\ D}{d_h} \tag{14}$$

$$Sh = 0.065\ Re^{0.875}\ Sc^{0.25} \tag{15}$$

$$Re = \frac{\rho_r\ v\ d_h}{\eta_r} \tag{16}$$

$$Sc = \frac{\eta_r}{\rho_r\ D} \tag{17}$$

To calculate the hydraulic diameter d_h and the cross-flow velocity v in spiral wound membranes, the procedure presented by Schock and Miquel can be used [28]. ρ_r and η_r stand for the density and the viscosity of the retentate. For diluted conditions, these values can be considered to be the same as for pure water. D is the bulk diffusion coefficient and can be calculated using the empirical relation proposed by Sano and Yamamoto in 1992 (Eq. 18), which links D_0 with the molecular weight of the sugar (Mw) [30].

$$D_0 = \frac{T}{9.5\ \cdot 10^{13} Mw^{1/3}\ \eta_{H2O}} \tag{18}$$

2.5 Mass transfer inside the membrane

While Φ represents the partitioning of a molecule at the interface of the membrane, the rejection represents the amount of solute that has been retained over the entire membrane thickness. To predict the rejection, the effect of the driving forces (pressure and concentration gradients) inside the membrane pore must be considered while taking into account the friction effect between the pore walls and the transient molecules. Bowen and Welfoot (2002) presented a modification of the SPM model that is briefly summarized as follows [5].

The flux of a component through the membrane (j) is the sum of the effect of convection, diffusion and pressure as shown in Eq. 19.

$$j = K_c C V - D_p \frac{dC}{dz} - \frac{C D_p}{RT} V_m \frac{dP}{dz} \tag{19}$$

The first term in Eq. 19 is the convection term in which K_c is the hindrance factor for convection, C is the local concentration and V is the solvent velocity inside the pore. The Hagen-Poisseuille relation describes the laminar flow of a liquid through a cylindrical tube, and can be used to estimate V as shown in Eq. 20, in which r_p represents the pore radius. Since $\Delta P = P_{per} - P_{ret}$, a negative sign should be included in this definition considering that ΔP is negative[1] in the direction of V.

$$V = \frac{r_p^2}{8\eta}\left(-\frac{\Delta P}{\Delta z}\right) = -\frac{r_p^2 \Delta P}{8\eta \Delta z} \tag{20}$$

The second term in Eq. 19 is the diffusion term, in which D_p is the diffusion coefficient inside the pore. To estimate it Eq. 21 can be used, in which the effect of the diffusion hindrance (Kd) and the increment in viscosity (η) due to the confinement of water is considered (Eq. 22). Here d is the thickness of the layer of water with increased viscosity that is estimated to be 0.28 nm.

$$D_p = K_d D \frac{\eta_0}{\eta} \tag{21}$$

$$\frac{\eta}{\eta_0} = 1 + 18\left(\frac{d}{r_p}\right) - 9\left(\frac{d}{r_p}\right)^2 \tag{22}$$

Many authors do not agree with this viscosity correction since there is not a physical proof of the accuracy of this relation. It can even be argued that the effects of this constriction are already accounted for by the hindrances coefficients. Studies in molecular dynamics do show that there is an effect on the water structure to constriction but the validity of Eq. 22 is certainly not yet proven [31-34]. Later on,

[1] This negative sign is mistakenly not considered in the original work of Bowen and Welfoot. This consideration affects the sign of 'Y' in Eq. 23.

however, it will be evident that this correction is irrelevant in the transport of neutral molecules because it cancels out in the definition of the Péclet number (Eq. 25).

The third term of Eq. 19 is the pressure effect in the transport. This is commonly the least important effect in membrane filtration processes. The V_m values can be calculated according to section 2.2.

After linearizing $\frac{dP}{dz}$ in Eq. 19, it can be rearranged and integrated over the thickness of the membrane, using the following boundary conditions: $z = 0$, $C = C_m\phi$ and $z = \Delta Z$, $C = C_p\phi$. Rearranging the terms and defining a new variable Y (Eq. 23), an expression for the Porewise Real Rejection $R_{(r)}$ can be obtained (Eq. 24) as function of a modified version of the Péclet number Pe' (Eq. 25).

$$Y = -\frac{D_P}{RT} V_m \frac{8\eta}{r_p^2} \tag{23}$$

$$R_{(r)} = 1 - \frac{(K_c - Y)\phi}{1 - [1 - (K_c - Y)\phi]\exp(-Pe')} \tag{24}$$

$$Pe' = -\frac{(K_c - Y)r_p^2}{8\eta D_p}\Delta P \tag{25}$$

Eq. 25 contains a negative sign which comes from the definition of V (Eq. 20). This sign cancels out with the negative value of ΔP, making Pe' a positive value. Additionally, the resulting value of Y is negative, which means that the effect of the pressure gradient on the transport of solutes is not opposed to convection as derived by Bowen and Welfoot [5], but goes in the same direction of the convective flow (Eq. 25).

$R_{(r)}$ is not the rejection of the whole membrane, but corresponds to one specific pore with pore radius r_p. To calculate the Overall Real Rejection R, the frequencies of the pore size distribution f_R should be considered as shown in Eq. 26 [35]. Here the effect of pore size on the viscosity inside the pore is also considered; however, its contribution is insignificant as the same consideration is made in the numerator and in the denominator.

$$R = \frac{\int_0^\infty \frac{f_R(r) r^4 R(r)}{\eta(r)} \mathrm{d}r}{\int_0^\infty \frac{f_R(r) r^4}{\eta(r)} \mathrm{d}r} \tag{26}$$

f_R can be calculated assuming a log normal distribution of the pore sizes as previously done in other NF and UF studies [5, 36-39]. As it is shown in Eq. 27, f_R is defined by two parameters: the mean radius r^* and the standard deviation σ. These two parameters can be estimated using data of R vs pressure obtained from experiments.

$$f_R(r) = \frac{1}{r\sqrt{2\pi b}} \exp\left\{ -\frac{\left[ln(r/r^*) + \frac{b}{2} \right]^2}{2b} \right\} \tag{27}$$

$$where\ b = \ln\left[1.0 + \left(\frac{\sigma^*}{r^*} \right)^2 \right]$$

2.6 Hindrance Coefficients

The hindrance to diffusion and convection originates from the combinations of particle – wall hydrodynamic interactions and steric restrictions [40]. For non-spherical molecules these interactions (drag and lag coefficients) are functions not only of position and molecular size, but also of orientation. This represent a challenge since all orientations must be averaged at all radial positions. Although the mathematical formulation is not complex, the information required is enormous [41].

Recently, Agasanapura et al. used computational fluid dynamics based on a centerline approximation to assess the convective hindrance in the filtration of capsular particles [19]. They found experimentally and with their model that convective hindrance was only relevant for small capsular particles ($\lambda < 0.4$) with small aspect ratio (closer to a sphere). For bigger molecules, the steric restrictions that limit the allowed positions and orientations dominate over the hydrodynamic particle-pore wall interactions, making the molecule travel at the average flow velocity [19]. Based on these findings and considering that the pore size of the membranes in this study is in the same order of magnitude as r_s of the sugars, K_c values become necessary only for molecules with DP lower than three. For molecules with a DP of

three or higher, $K_c = 1$ can be considered. The following expression for K_c can be used considering $\lambda = r_G/r_p$ [40].

$$K_c = \frac{1 + 3.867\lambda - 1.907\lambda^2 - 0.834\lambda^3}{1 + 1.867\lambda - 0.741\lambda^2} \tag{28}$$

In the case of the calculation of K_d for non-spherical molecules, to the best of our knowledge nothing concrete has been achieved yet. Even the assumption that rotational Brownian motion is sufficient to ensure complete randomness of solute orientation is uncertain. Randomness can only be assured when the rotational diffusivity of the solute is higher than the vorticity of the velocity field in the pore [41]. There are some theoretical studies that calculate the hindrances for polymer coils in cylindrical pores, by considering these macromolecules to be solvent-permeable bodies determining a permeability distribution across the pore [42]; however, in our case it does not seem appropriate to approximate rigid molecules to porous bodies. We believe instead that is safer to make use of the available theory for rigid spheres as done by other researchers when investigating the transport of elongated molecules [13, 43]. An expression for K_d applicable to any λ value from 0 to 1 can be obtained from the work of Bungay and Brenner (1973) [44]. Calculating λ using r_s ensures consistency with the fact that Stokes' law was considered in the estimation of the drag force by Bungary and Brenner [44, 45].

$$K_d(\lambda) = \frac{6\pi}{K_t(\lambda)} \tag{29}$$

$$K_t(\lambda) = \frac{9}{4}\pi^2\sqrt{2}\,(1-\lambda)^{-\frac{5}{2}}\left[1 + \sum_{n=1}^{2} a_n(1-\lambda)^n\right] + \sum_{n=0}^{4} a_{n+3}\,\lambda^n$$

$$a_1 = -1.2167, a_2 = 1.533, a_3 = -22.5083, a_4 = -5.6117, a_5 = -0.3363,$$

$$a_6 = -1.216, a_7 = 1.647$$

3. Materials and methods

3.1 Chemicals

Demineralised water was used in every experiment. In the case of the simple sugars, xylose was purchased from Merck KGaA (Darmstadt, Germany) and glucose, fructose, sucrose and raffinose pentahydrate were purchased from Sigma-Aldrich (Munich-Germany). The fructooligosaccharides (FOS) mixture Frutalose® L85 (batch: 8554908001) was kindly provided by Sensus (Roosendaal, Netherlands). This mixture is a viscous, clear syrup with a concentration of 75% w/w, composed by mono, di and oligo-saccharides up to a DP of 10. Its composition on dry basis is shown in Table 2.

Table 2. Composition of fructooligosaccharides mixture (Frutalose® L85) on dry basis

Component	% (w/w)
DP1	6.1
DP2	7.6
DP3	28.8
DP4	22.5
DP5	16.9
DP6	12.2
DP7	5.2
DP8*	0.3
DP9*	0.4
DP10*	0.2

DP = Degree of polymerization.

* Molecules that were not considered in the mathematical modelling.

Although the DP of the oligosaccharide mixture ranged from 1 to 10, only data up to DP7 was considered for the calculations and modelling since the concentrations of the higher DP molecules were too small to be measured accurately.

3.2 Membrane

A thin film composite (thin polyamide layer deposited on top of polysulfone porous layer), spiral wound GE membrane (GE Osmonics, Sterlitech, Kent – WA, United States) was used for all the experiments. This UF membrane was chosen mainly due to its appropriate MWCO and its good resistance to high temperatures as shown in Table 3. The experiments were performed in a pilot scale filtration system that included heat exchangers in the feed tank and in the recirculation loop of the retentate. The flow, temperature and pressure of both retentate and permeate streams were monitored by computer (DDE software from Labview).

Table 3. Specifications of GE membrane

Membrane specifications	GE
Model	1812C-34D
Type	Spiral wound
Manufacturer	General Electric
Membrane material	TFM
MWCO (declared by manufacturer)	1000 Da
Membrane area	0.32 m^2
Permeability at 45° C*	7.06 x 10^{-12} m/(Pa s)
Spacer height*	8.60 x 10^{-4} m
Spacer porosity*	0.93
Maximum temperature	50°C

* Membrane characteristics measured in our lab.

3.3 Estimation of pore size distribution

The pore size distribution of the GE membrane was determined by estimating the parameters $r^*$and σ. These two parameters were fitted making use of the equations presented in section 2.4 and 2.5 and experimental rejection data obtained from filtration experiments with oligosaccharides. During this experiments, a very diluted aqueous solution (0.5% w/w) of Frutalose® L85 was used as feed to avoid osmotic pressure effects. The retentate and the permeate streams were recycled back to the feed tank,

and once the system reached steady state (constant permeate flux), samples were taken from both streams simultaneously. This operation was repeated at many pressures (2.5 – 20 bar). All runs were performed at 45°C to mimic industrial conditions and avoid microbial growth. The retentate recirculation flow was 150 L/h with a crossflow velocity of 0.088 m/s in the membrane module.

Using the collected data and process parameters, experimental R values for each molecule were calculated with Eqs. 11-18. As a result, 7 experimental curves of R vs Pressure (one for each DP), can be obtained. $r^*$and σ were fitted using all these curves simultaneously, considering that even when the sizes of the molecules were different, the pore size distribution is the same because all the experiments were performed with the same GE membrane. The sizes of the molecules were calculated according to the three different approaches for the calculation of the species radii presented in section 2.1: (1) Spherical (r_S), (2) Simplified Capsular (r_G) and (3) Complete Capsular (r_1, r_0). In each case, modelled R was obtained by solving the Eqs. 21-29. After an iterative procedure, it was determined which values for the parameters $r^*$and σ produce the best description.

3.4 Analytical methods

The concentration of simple sugars was measured using High Performance Liquid Chromatography. A Shodex column KS-806 was used at 80°C with MilliQ water as eluent at a flow rate of 1mL/min. The detection was performed with a RI detector (Shodex R9-101). For the oligosaccharides mixture, an Ion Exchange Chromatography technique was used based on the method of Campbel et al. (1997) [24]. The Dionex column Carbopac PA-100, 250 x4.6mm + guard was utilized at 20°C. Three eluents were used: Demineralised water, 0.25M NaOH and 0.65M NaOAc at a flow rate of 1mL/min. The detection was performed with an electrochemical detector (Dionex ED-40, range 500 nC, pulse train 2).

3.5 Computational analysis

MATLAB R2015b was used for all the calculations. For the simultaneous fitting of two parameters the function ‘lsqcurvefit’ was used. This function solves nonlinear curve-fitting problems in least squares

sense using the 'trust-region-reflective' algorithm. For the resolution of Eqs. 7, 8 and 26, the expressions were numerically integrated using the function 'integral'.

4. Results and discussion

4.1 Calculation of the partition coefficient

Only neutral molecules (sugars) were used as solutes in this study and it was assumed that no interaction occurred between the solutes and the membrane; consequently, the partitioning of these molecules in the membrane is determined solely by steric effects. The shape and size of the FOS molecules were estimated according to three different approaches: (1) Using the Stokes equation, in which the hydrodynamic radius (r_S) is calculated assuming an spherical molecular shape; (2) using the Simplified Capsular approach in which an average radius (r_G) is calculated; and (3) using the Complete Capsular approach considering 2 dimensions to represent this capsular shape (r_1, r_0).

Figure 4 shows the Φ values for all FOS molecules considering a hypothetical pore radius of 2 nm. As described by Giddings et al., the Φ values calculated using r_G were very similar to those calculated using the Complete Capsular approach (r_1, r_0). Conversely, Φ values calculated with r_S were consistently higher than the ones obtained with the other two methods. This was expected considering the fact that, for the FOS molecules, r_S was smaller than r_G (Figure 3). In the case of the DP1 sugar, since it is a spherical molecule, a similar Φ was obtained with all the approaches.

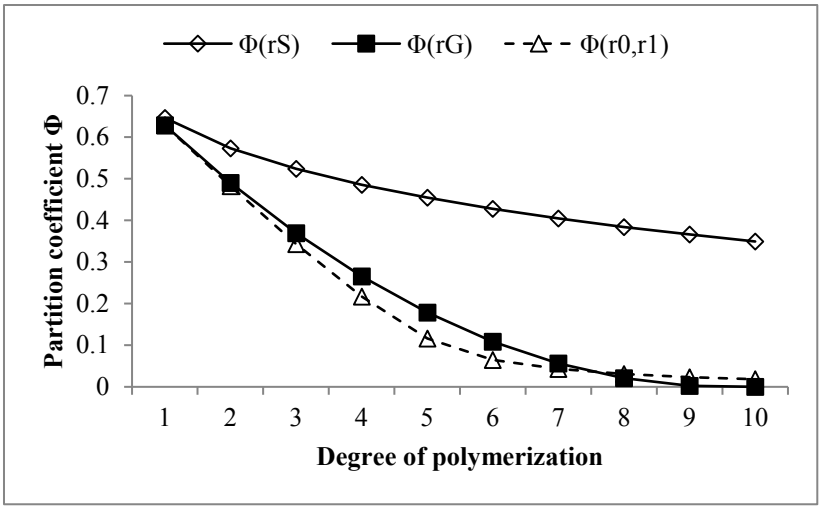

Figure 4. Partition coefficients for fructooligosaccharides with a degree of polymerization up to 10. Three approaches were used with respect to the molecular shape and size estimation: Spherical ($\boldsymbol{r_S}$), Simplified Capsular ($\boldsymbol{r_G}$) and Complete Capsular ($\boldsymbol{r_0}$,$\boldsymbol{r_1}$). The pore radius used in this calculation was 2 nm. Only the symbols are produced by the calculations; lines were drawn to guide the eye.

r_G is a good empirical approximation that simplifies the calculation of Φ greatly. It produces slightly higher values than the Complete Capsular approach when r_G/r_p is between 0.4 and 0.6, and slightly lower values when Φ is close to zero. This curious similarity between these two methods was assessed in Figure 5, in which Φ is illustrated as the ratio between the area available for the centre of the molecule in the pore and the total pore area. The calculations for this figure were made considering a DP4 molecule entering a pore of r_p=2 nm.

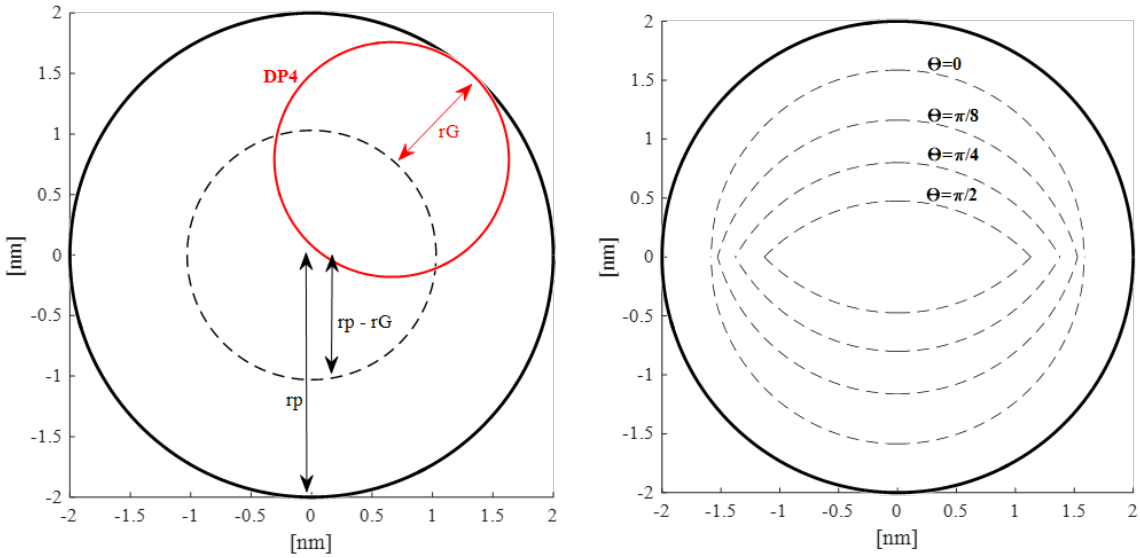

Figure 5. Comparison between the Simplified Capsular (left) and the Complete Capsular (right) approaches for the Φ calculation of a DP4 molecule in a pore with a 2 nm radius. Left: The area surrounded by the dashed line is the area available for the centre of the spherical molecule of radius r_G. Right: The area surrounded by the dashed lines represent the available area for the centre of a capsular molecule at different orientation angles θ.

Figure 5 (left) illustrates the calculation of Φ according to the Simplified Capsular approach in which r_G is used to represent the molecular size (Eq. 10). The area surrounded by the dashed line is the area available for the centre of the spherical molecule of radius r_G, while the area outside this line is the area that is excluded due to steric effects with the wall. The ratio between the available area and the total pore area is equal to Φ. Molecular orientation here is not relevant, since the molecule is considered spherical for the Φ calculation. It is clear that as soon as r_p is equal or smaller than r_G, Φ becomes zero, which means that the molecule is totally excluded from the pore. Likewise, the calculation of Φ with the Complete Capsular approach is represented in Figure 5 (right), in which dashed lines surround the available area for the centre of capsular molecules at specific orientation angles θ. The ratios between these areas with the total pore area are equivalent to local partition coefficients φ'' as represented in Eq. **5**, while the global partition coefficient Φ is the configuration-space average of these local values (Eq. 3). As expected, when the axis of the pore and that of the capsule are aligned ($\theta = 0$), φ'' is the highest for a given molecule since its projected area in the pore plane is the smallest possible. As consequence, the available area for the molecule is then the greatest

possible, resulting in a lower probability to touch the wall compared with other orientations. As θ increases, the projected area becomes larger, decreasing the available area for the molecule and its φ'' value. This explains the difference between both methods when Φ is close to zero in Figure 4. With the Simplified Capsular approach, as soon as a r_G is equal to r_p, Φ becomes zero, while in reality some molecular orientations still allow the entrance of the molecule in the pore when the axis of the pore and the molecule are aligned ($\theta \rightarrow 0$). This latter situation is adequately represented by the Complete Capsular approach. By using this method, it can be verified that for capsular molecules of similar volume, the greater the aspect ratio, the lower Φ, being the spherical conformation always the more compact, so the one with the highest Φ value.

4.2 Pore size distribution estimation

The pore size distribution of the GE membrane was estimated by using the model presented in sections 2.4 -2.6 to fit two parameters (r^* and σ) to experimental rejection data. This operation was repeated using the three different methods for the molecular size and shape estimation according to section 2.1.

In the case of the Simplified and Complete Capsular approaches, the fitting procedure worked fine and the model output matches the experimental measurements as shown in Figure 6. At low pressures, nevertheless, in the range where diffusion is an important driving force, the modelled rejection was systematically higher than the experimental data. For these two approaches the modelled rejection reached a plateau at lower pressures than the experimental data, meaning that the diffusion mechanism is underestimated in the model. We believe that the way how K_d was calculated (using r_s) slightly overestimates the effect of diffusion hindrance, producing K_d values lower than real, which result in higher rejections. An observation that supports this explanation is the better agreement between the model and the measurements for the DP1 molecules, which actually have a r_s radius. In the case of the oligosaccharides (elongated molecules), their orientation influences their interaction with the pore wall, thus K_d would be a complex function of r_1, r_0 and r_p. It is also expected that K_d would be lower for longer chains, as its movement inside the pore is more limited.

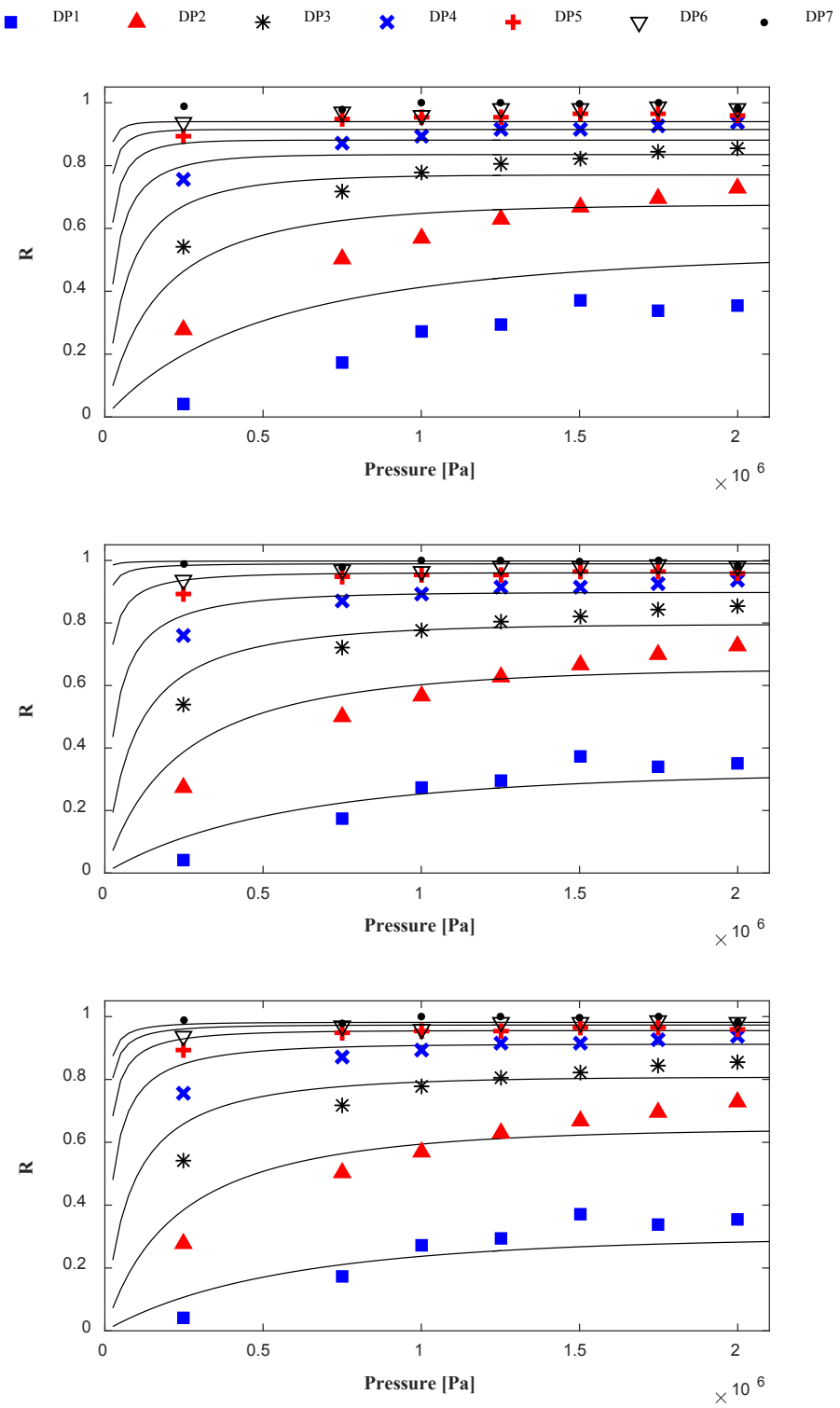

Figure 6. FOS rejections according to the Spherical (top), Simplified Capsular (middle) and Complete Capsular (bottom) approaches. The fitting procedures in all cases were done with the same experimental data, represented by symbols. Lines represent the output of the model using the estimated parameters for each case (see Table 4).

In the case of the Spherical approach, the resulting fit is not accurate for low and high rejection values as it is shown in the Figure 6 (top). The r_S values of DP1 to DP7 molecules scarcely differ from each other (Figure 3), resulting in a relatively narrow spectrum of rejections compared with the experimental results. Somewhat similar results were obtained by Nakao and Kimura when estimating the pore size of a UF membrane using different solutes [46]. They found that a linear polymer (PEG#4000) gave inconsistent results (too large pore size) when considering its r_S in the model. We are proving here that by considering the right solute shape, a unique pore size distribution can be estimated from rejection data, regardless the size of the solute molecules. Some authors argue that different solutes result in different pore sizes due to the tortuosity of the membrane. In our case, it was not necessary to incorporate more parameters to obtain a good description of the rejection data.

Table 4 shows the results of the parameter estimation procedure. It was found that the results obtained using the Simplified and Complete Capsular approaches were consistent with each other, while the Spherical approach resulted in a pore size distribution with a much lower r^* value. This was expected considering that r_S was much smaller than r_G and r_1 (Figure 3). Additionally, the effectiveness of the fitting, reflected in the sum of the squares of the errors E, was much better for the Simplified and Complete Capsular approaches.

Table 4. Comparison of the parameter estimation results for the pore size distribution of the GE membrane.

Method	Estimated parameters [nm]		$\boldsymbol{E}$	Accuracy	
	r^*	σ		s_{r^*} (CV_{r^*})	s_σ (CV_σ)
Spherical	0.94	0.010	0.366	0.10 (0.11)	3.78 (»1)
Simplified Capsular	1.29	0.17	0.082	0.09 (0.07)	0.07 (0.41)
Complete Capsular	1.31	0.21	0.097	0.07 (0.05)	0.11 (0.52)

r^*= Mean radius, σ= Std. deviation of the pore size distribution, , E= Sum of the square of the errors, s= Std. deviation of the estimated parameters, CV= Coefficient of variation.

To evaluate the accuracy of the non-linear fitting, also indicated as the estimation uncertainty, the standard deviation (s) of the estimated parameters was calculated for all three approaches (Table 4)

[47]. Likewise, the coefficient of variation (CV), which is the ratio of the standard deviation to the estimated parameter, was calculated in every case.

For the spherical approach, it was found that the s_σ value was higher than the estimated σ,which means that σ for this approach cannot be accurately estimated. For the other 2 approaches (Simplified and Complete Capsular), the CV values were much lower. In general, the fitting procedure allowed a more accurate estimation of r^* than σ. Nevertheless, the estimated σ values for the Simplified and Complete Capsular approach were found acceptable as their CV was not excessively high.

Since it is a non-linear fitting, confidence intervals cannot be used [47]. Instead, Draper and Smith suggest to define a confidence region, delimited with contour lines of equal E, that can be viewed as 'equally likely' [48]. As example, we show in Figure 7 these contour lines for the case of the Simplified Capsular approach, in which a correlation between the parameters can be seen. This means that during the parameters estimation, a change in one parameter can be partially compensated by a change in the other parameter. In our case, an increase in σ can be compensated by a decrease in r^* and vice versa. Under these circumstances, it is critical to use solutes with a size comparable to that of the pore (as done in this study), to make their rejection more sensitive to changes in the parameters that define the pore size distribution of the membrane. A plot similar to Figure 7 was also obtained for the Complete Capsular approach.

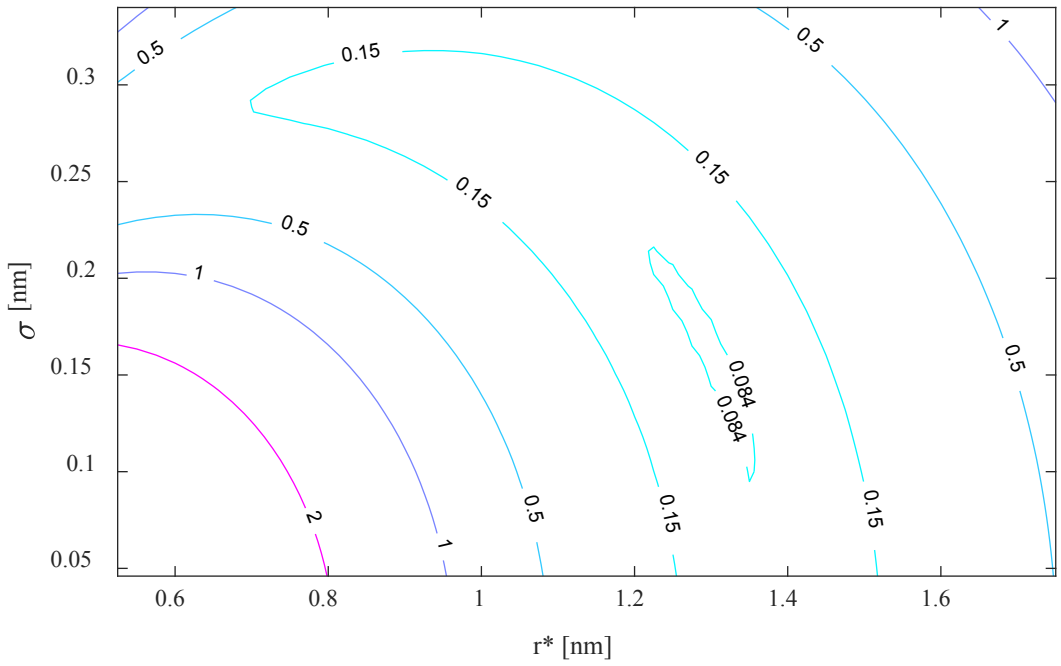

Figure 7. Contour plot of the sum of the squares of the errors (***E***) as function of the two estimated parameters: $\boldsymbol{r}^*$ and $\boldsymbol{\sigma}$. Results belong to the Simplified Capsular approach.

The estimation of pore size distributions using rejection data has the disadvantage that rejection depends on r^4 (Eq. 26). This dependency means that the pore size estimation is very sensitive to few larger pores. Thus, sometimes diffusive data is preferred, because then the dependency is only on r^2. Nevertheless, realistic pore size distributions were obtained using the Simplified and the Complete Capsular approaches. While these results are consistent with each other; the computer resources for the calculation were much higher for the Complete Capsular approach, which resulted in a slightly wider (higher σ value) pore size distribution as it is shown in Figure 8.

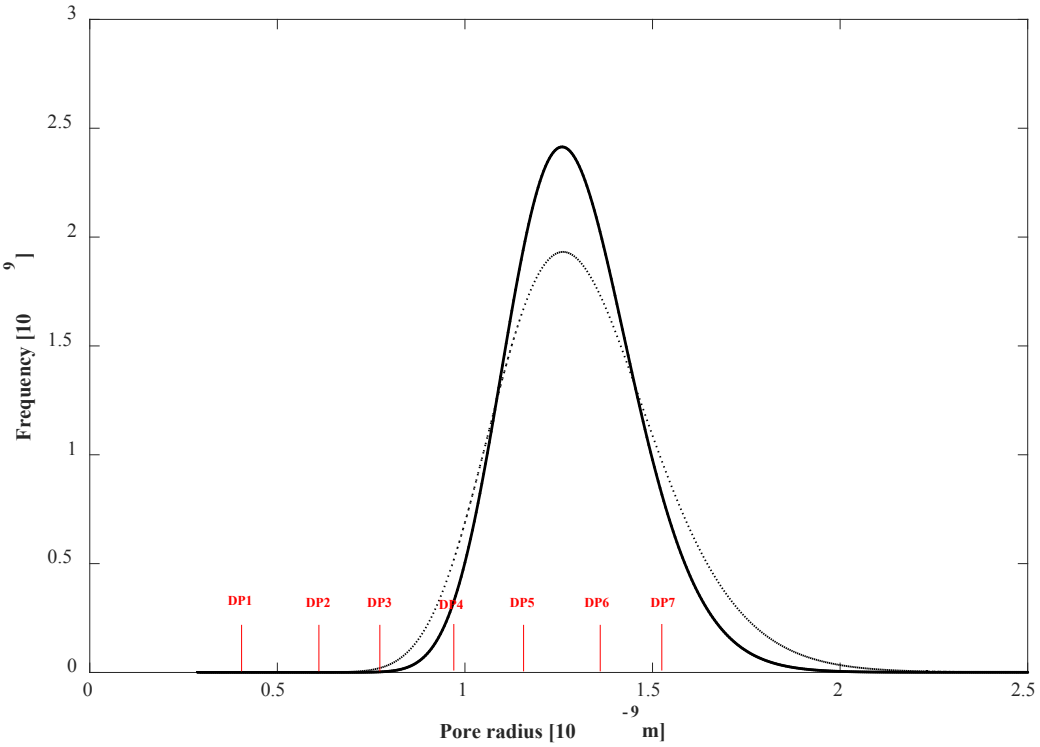

Figure 8. Pore size distribution estimated according to the Simplified Capsular (continuous line) and the Complete Capsular (dotted line) approaches. r_G values of the oligosaccharide molecules are shown in the x axis.

Figure 8 shows that the size of the pores of the GE membrane are in the same order of magnitude as the r_G of the FOS molecules. This demonstrates how critical a good estimation of the pore size distribution is for this type of purification processes. Even when the r_G values for DP6 and DP7 molecules are smaller than a fraction of pores in the membrane, the rejection for these molecules is practically 1 because the few molecules that enter the pore are slowed down by the hindrance inside the pore. Frequently, these steric and hydrodynamic interactions inside the pore are not included in characterization studies, in which only data at limiting conditions (high flux) is considered for the fitting of the pore size distribution. The resulting drawback is the small number of degrees of freedom (number of measurements – number of estimated parameters), which might make the estimation statistically insignificant. Considering the fact that Φ is relevant at limiting conditions, the molecular shape considerations should always be included in this type of studies.

4.3 Model validation

To check the validity of the model, the estimated pore size distributions were utilized to predict the rejection of different sugars in a new set of experiments using the same GE membrane. Single diluted solutions (0.2% w/w) of raffinose, sucrose, and xylose were utilized as feed at 45°C with a crossflow velocity of 0.088 m/s. Their dimensions were estimated as explained in previous sections. Using the estimated values for $r^*$and σ, the R values for these sugars were predicted and compared with experimental data. Figure 9 shows the comparison between the predicted rejections calculated using all three approaches and the experimental measurements.

In the case of the Simplified and Complete Capsular Approach, the accuracy of the predictions is good, although both methods tend to slightly underestimate the rejection of raffinose. This might be due to inaccuracies in the size estimation of raffinose since we assumed that two of its monomers, glucose and galactose, have the same size. In the case of xylose, the difference in the predictions is entirely due to the different pore size distribution used with each method. Both methods are equivalent in this case because xylose is a monomer and is considered a sphere, thus $r_1 = r_0 = r_G$. Since the Complete Capsular approach resulted in a wider pore size distribution and considering that bigger pores have a greater effect in the rejection, the predicted rejection for xylose is slightly lower than the one calculated with the Simplified Capsular approach. For bigger molecules (sucrose and raffinose) this trend changed and the rejection predictions of the Complete Capsular approach became higher than that of the Simplified Capsular approach. This is expected considering that in this range of λ values, Φ are slightly smaller when calculated using the Complete Capsular approach.

The Spherical approach overestimates the rejection of xylose and greatly underestimates the rejection of raffinose. As expected, the prediction cannot cover the entire spectrum of rejections due to the relatively small difference in the r_S of the sugars. In the case of xylose, even when all three approaches are similar for spherical molecules, the prediction of the Spherical approach is the worst due to the incorrect pore size distribution obtained in the previous section.

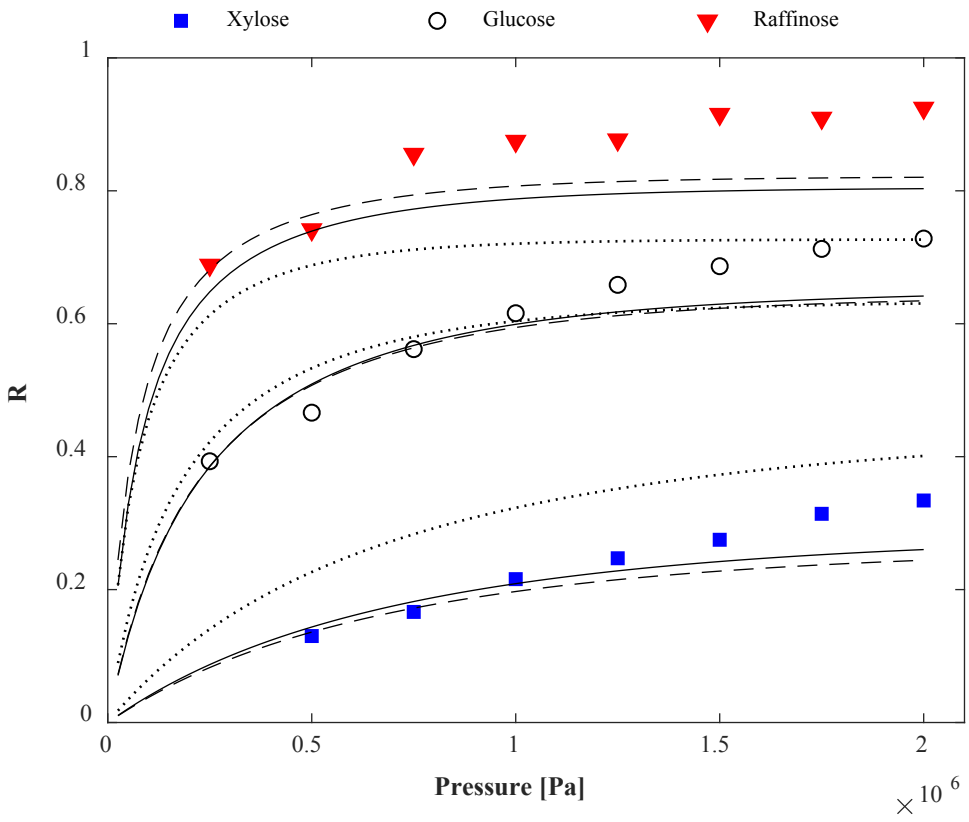

Figure 9 Comparison of the R predictions using the Spherical (dotted lines), Simplified Capsular (continuous lines) and the Complete Capsular (dashed lines) approaches. The pore size distributions used here were the ones obtained previously with each method (shown in Table 4).

5. Conclusions

The ultrafiltration of rigid elongated molecules was assessed for modelling purposes. Three different strategies for the representation of the molecular size were evaluated: Spherical approach, Simplified Capsular approach and Complete Capsular approach. It was demonstrated that considering elongated molecules to be capsule-shaped gives better predictions of the rejection of rigid neutral molecules such as oligosaccharides.

The capsular shape is preferred over other geometries because it can be represented by only two parameters, making the calculation of its partition in cylindrical pores straightforward. In addition, the capsule dimensions of oligomers can be easily inferred from the dimensions their monomers in the case of rigid-chain molecules.

Both the Simplified and Complete Capsular approaches satisfactorily predicted the rejection of sugars of different sizes at different pressures. Due to its simplicity and lower computing power demand, we suggest to use the Simplified Capsular approach for pore size estimation and rejection prediction, unless higher accuracy is needed (especially at high R values); in that case, we suggest to use the Complete Capsular approach.

A proper method for the calculation of the diffusion hindrance inside the pore (K_d) remains as a challenge for elongated molecules. In this study, this parameter was roughly estimated using an spherical approximation for the shape of the molecule. It was observed that the effect of K_d is relevant at low pressures in the range where diffusion is a significant transport mechanism inside the pores.

6. Acknowledgements

This work was carried out as part of a project of the Institute for Sustainable Process Technology, The Netherlands: project number CM-20-05.

Nomenclature

C	Concentration [mol/m^3]
C_c	Correlation coefficient [dimensionless]
Cov	Covariance matrix [m^2]
D	Diffusion coefficient [m^2/s]
D_p	Diffusion coefficient inside the pore[m^2/s]
d	Diameter of the water molecule [m]
d_h	Hydraulic diameter [m]
E	Sum of the squares of the errors [dimensionless]
f_R	Frequency [dimensionless]
J	Permeate flux [m/s]
Jac	Jacobian Matrix [m^{-1}]
K_c	Hindrance coefficient for convection [dimensionless]
K_d	Hindrance coefficient for diffusion [dimensionless]
k	Mass transfer coefficient [m/s]
k_B	Boltzmann constant [J/K]
L_p	Permeability
L_1	Length of the capsular molecule [m]
L_0	Width and depth of the capsular molecule [m]
Mw	Molecular weight [g/mol]
N	Number of measurements [dimensionless]
n_H	Hydration number [dimensionless]
n_p	Number of estimated parameters [dimensionless]
P	Pressure [Pa]
p	Position [m]
q	Probability of no intersection with pore walls [dimensionless]
R	Real rejection Eqs. 12 and 26
R	Gas constant [J/(K mol)] Eqs. 19 and 23

Re	Reynolds number [dimensionless]
r_G	Average radius according to the Simplified Capsular approach [m]
r_i	Radius of molecule i [m]
r_p	Radius of the pore [m]
r_S	Stokes' radius [m]
r_1	Half of the capsular length [m]
r_0	Radius of the caps of the capsule [m]
r^*	Mean radius [m]
$\widehat{r_p}$	Radius of the pore for the infinitely thin rod approximation [m]
$\widehat{r_1}$	Half of the length of the rod for the infinitely thin rod approximation [m]
Sc	Schmidt number [dimensionless]
Sh	Sherwood number [dimensionless]
T	Temperature [K]
V	Pore wise flow velocity [m/s]
V_m	Molar volume [m^3/mol]
v	Cross flow velocity [m/s]

Greek letters

η	Viscosity [Pa s]
θ	Angle between the axis of the capsular molecule and the axis of the pore [rad]
λ	Ratio between the molecular and pore radii [dimensionless]
ρ	Density [Kg/m^3]
σ	standard deviation of the pore size distribution [m]
Φ	Global partition coefficient [dimensionless]
φ'	Local partition coefficient as function of position [dimensionless]
φ''	Local partition coefficient as function of orientation [dimensionless]
ψ	Orientation [rad]

REFERENCES

[1] R. Baker, Membrane Technology and Applications 2nd ed., Wiley, California, USA, 2004.
[2] O. Kedem, A. Katchalsky, Thermodynamic analysis of the permeability of biological membranes to non-electrolytes, Biochim. Biophys. Acta, 27 (1958) 229-246.
[3] K. Spiegler, O. Kedem, Thermodynamics of hyperfiltration (reverse osmosis): criteria for efficient membranes, Desalination, 1 (1966) 311-326.
[4] W.R. Bowen, A.W. Mohammad, Characterization and Prediction of Nanofiltration Membrane Performance—A General Assessment, Chem. Eng. Res. Des., 76 (1998) 885-893.
[5] W.R. Bowen, J.S. Welfoot, Modelling the performance of membrane nanofiltration—critical assessment and model development, Chem. Eng. Sci., 57 (2002) 1121-1137.
[6] V. Silva, P. Prádanos, L. Palacio, J.I. Calvo, A. Hernández, Relevance of hindrance factors and hydrodynamic pressure gradient in the modelization of the transport of neutral solutes across nanofiltration membranes, Chem. Eng. J., 149 (2009) 78-86.
[7] B. Van der Bruggen, J. Schaep, D. Wilms, C. Vandecasteele, Influence of molecular size, polarity and charge on the retention of organic molecules by nanofiltration, J. Membr. Sci., 156 (1999) 29-41.
[8] V.N. Tsvetkov, Molecular structure and physical properties of rigid chain polymers in solutions. Review, Polymer Science U.S.S.R., 25 (1983) 1815-1835.
[9] T. Norisuye, M. Motowoka, H. Fujita, Wormlike Chains Near the Rod Limit: Translational Friction Coefficient, Macromolecules, 12 (1979) 320-323.
[10] I. Teraoka, K.H. Langley, F.E. Karasz, Reptation dynamics of semirigid polymers in porous media, Macromolecules, 25 (1992) 6106-6112.
[11] B. Van der Bruggen, C. Vandecasteele, Modelling of the retention of uncharged molecules with nanofiltration, Water Res., 36 (2002) 1360-1368.
[12] Y. Kiso, K. Muroshige, T. Oguchi, M. Hirose, T. Ohara, T. Shintani, Pore radius estimation based on organic solute molecular shape and effects of pressure on pore radius for a reverse osmosis membrane, J. Membr. Sci., 369 (2011) 290-298.
[13] Y. Kiso, K. Muroshige, T. Oguchi, T. Yamada, M. Hhirose, T. Ohara, T. Shintani, Effect of molecular shape on rejection of uncharged organic compounds by nanofiltration membranes and on calculated pore radii, J. Membr. Sci., 358 (2010) 101-113.
[14] J.L.C. Santos, P. de Beukelaar, I.F.J. Vankelecom, S. Velizarov, J.G. Crespo, Effect of solute geometry and orientation on the rejection of uncharged compounds by nanofiltration, Sep. Purif. Technol., 50 (2006) 122-131.
[15] F. Vinther, M. Pinelo, M. Brøns, G. Jonsson, A.S. Meyer, Statistical modelling of the interplay between solute shape and rejection in porous membranes, Sep. Purif. Technol., 89 (2012) 261-269.
[16] J.C. Giddings, E. Kucera, C.P. Russell, M.N. Myers, Statistical theory for the equilibrium distribution of rigid molecules in inert porous networks. Exclusion chromatography, The Journal of Physical Chemistry, 72 (1968) 4397-4408.
[17] E.M. Renkin, Filtration, diffusion, and molecular sieving through porous cellulose membranes, The Journal of general physiology, 38 (1954) 225-243.
[18] W. Sutherland, LXXV. A dynamical theory of diffusion for non-electrolytes and the molecular mass of albumin, The London, Edinburgh, and Dublin Philosophical Magazine and Journal of Science, 9 (1905) 781-785.
[19] B. Agasanapura, R.E. Baltus, C. Tanneru, S. Chellam, Membrane rejection of nonspherical particles: Modeling and experiment, AlChE J., 59 (2013) 3863-3873.
[20] A. Almond, Towards understanding the interaction between oligosaccharides and water molecules, Carbohydr. Res., 340 (2005) 907-920.
[21] A. Gharsallaoui, B. Rogé, J. Génotelle, M. Mathlouthi, Relationships between hydration number, water activity and density of aqueous sugar solutions, Food Chem., 106 (2008) 1443-1453.
[22] A. Almond, A. Brass, J.K. Sheehan, Oligosaccharides as Model Systems for Understanding Water−Biopolymer Interaction: Hydrated Dynamics of a Hyaluronan Decamer, The Journal of Physical Chemistry B, 104 (2000) 5634-5640.
[23] A. Almond, B.O. Petersen, J.Ø. Duus, Oligosaccharides Implicated in Recognition Are Predicted to Have Relatively Ordered Structures, Biochemistry, 43 (2004) 5853-5863.

[24] J.M. Campbell, L.L. Bauer, G.C. Fahey, A.J.C.L. Hogarth, B.W. Wolf, D.E. Hunter, Selected Fructooligosaccharide (1-Kestose, Nystose, and 1F-β-Fructofuranosylnystose) Composition of Foods and Feeds, J. Agric. Food. Chem., 45 (1997) 3076-3082.
[25] G. Lelong, W.S. Howells, J.W. Brady, C. Talón, D.L. Price, M.-L. Saboungi, Translational and rotational dynamics of monosaccharide solutions, The Journal of Physical Chemistry B, 113 (2009) 13079-13085.
[26] W.H. Brown, T. Poon, T. Poon, Introduction to organic chemistry, John Wiley & Sons, 2014.
[27] H. Shiio, Ultrasonic interferometer measurements of the amount of bound water. Saccharides, J. Am. Chem. Soc., 80 (1958) 70-73.
[28] G. Schock, A. Miquel, Mass transfer and pressure loss in spiral wound modules, Desalination, 64 (1987) 339-352.
[29] V. Geraldes, A.M. Brites Alves, Computer program for simulation of mass transport in nanofiltration membranes, J. Membr. Sci., 321 (2008) 172-182.
[30] Y. Sano, S. Yamamoto, Mutual Diffusion Coefficient of Aqueous Sugar Solutions, J. Chem. Eng. Jpn., 26 (1993) 633-636.
[31] I. Brovchenko, A. Geiger, A. Oleinikova, D. Paschek, Phase coexistence and dynamic properties of water in nanopores, The European Physical Journal E, 12 (2003) 69-76.
[32] P. Hirunsit, P.B. Balbuena, Effects of Confinement on Water Structure and Dynamics: A Molecular Simulation Study, The Journal of Physical Chemistry C, 111 (2007) 1709-1715.
[33] A.I. Kolesnikov, J.-M. Zanotti, C.-K. Loong, P. Thiyagarajan, A.P. Moravsky, R.O. Loutfy, C.J. Burnham, Anomalously Soft Dynamics of Water in a Nanotube: A Revelation of Nanoscale Confinement, Phys. Rev. Lett., 93 (2004) 035503.
[34] R. Mancinelli, The effect of confinement on water structure, J. Phys.: Condens. Matter, 22 (2010) 404213.
[35] W.R. Bowen, J.S. Welfoot, Modelling of membrane nanofiltration—pore size distribution effects, Chem. Eng. Sci., 57 (2002) 1393-1407.
[36] P. Aimar, M. Meireles, V. Sanchez, A contribution to the translation of retention curves into pore size distributions for sieving membranes, J. Membr. Sci., 54 (1990) 321-338.
[37] N. García-Martín, V. Silva, F. Carmona, L. Palacio, A. Hernández, P. Prádanos, Pore size analysis from retention of neutral solutes through nanofiltration membranes. The contribution of concentration–polarization, Desalination, 344 (2014) 1-11.
[38] S. Mochizuki, A.L. Zydney, Theoretical analysis of pore size distribution effects on membrane transport, J. Membr. Sci., 82 (1993) 211-227.
[39] A.L. Zydney, P. Aimar, M. Meireles, J.M. Pimbley, G. Belfort, Use of the log-normal probability density function to analyze membrane pore size distributions: functional forms and discrepancies, J. Membr. Sci., 91 (1994) 293-298.
[40] P. Dechadilok, W.M. Deen, Hindrance Factors for Diffusion and Convection in Pores, Industrial & Engineering Chemistry Research, 45 (2006) 6953-6959.
[41] J.L. Anderson, J.A. Quinn, Restricted Transport in Small Pores: A Model for Steric Exclusion and Hindered Particle Motion, Biophys. J., 14 (1974) 130-150.
[42] M. G. Davidson, W. M. Deen, Hydrodynamic theory for the hindered transport of flexible macromolecules in porous membranes, J. Membr. Sci., 35 (1988) 167-192.
[43] V. Silva, P. Prádanos, L. Palacio, A. Hernández, Alternative pore hindrance factors: What one should be used for nanofiltration modelization?, Desalination, 245 (2009) 606-613.
[44] P.M. Bungay, H. Brenner, The motion of a closely-fitting sphere in a fluid-filled tube, Int. J. Multiphase Flow, 1 (1973) 25-56.
[45] W. Deen, Hindered transport of large molecules in liquid-filled pores, AlChE J., 33 (1987) 1409-1425.
[46] S.-I. Nakao, S. Kimura, ANALYSIS OF SOLUTES REJECTION IN ULTRAFILTRATION, J. Chem. Eng. Jpn., 14 (1981) 32-37.
[47] K.J. Keesman, System identification: an introduction, Springer Science & Business Media, 2011.
[48] N.R. Draper, H. Smith, Applied Regression Analysis, Wiley, New York, 1966.